Mechanical behaviour of Lixhe chalk partly saturated by oil and water: experiment and modelling

F. Collin[1,*,†], Y. J. Cui[2], C. Schroeder[3] and R. Charlier[1]

[1] *Departement MSM, University of Liège, Liege, Belgium*
[2] *CERMES, Ecole Nationale des Ponts et Chaussées, France*
[3] *Departement LGIH, University of Liège, Belgium*

SUMMARY

Two or more different fluids generally saturate chalk in oil reservoir, and therefore its behaviour can be very complicated. In this paper, a constitutive law is proposed for modelling the mechanical behaviour of a chalk saturated by two non-miscible fluids, water and oil. The effects of the capillary pressure or suction are taken into account. They are considered as an independent variable, as in the Barcelona's basic model developed for unsaturated soils. On the other hand, internal friction and pore collapse are modelled as independent mechanisms. The determination of the parameters is based on triaxial and oedometer tests. Finally, in order to validate the model, predictions are compared with experimental results of water-flooding test. Copyright © 2002 John Wiley & Sons, Ltd.

KEY WORDS: chalk compaction; suction; water-flooding tests; multisurface plasticity; numerical modelling

1. INTRODUCTION

Chalk is the constituent material of numerous oil reservoirs in North Sea. This soft rock is composed of assemblies of coccolithe skeletons (unicellular organism) or pieces of skeleton. Due to its geological history [1,2], the chalk is partly saturated by oil and water (and sometimes by gas also). Initially, chalk deposited in marine environment was saturated by seawater and during geological time, oil migrated and progressively intruded the pores, remaining some residual water menisci at inter-granular contacts.

Ekofisk is one of the main oilfields in North Sea, which is located 200 km west of the Norwegian coasts. Exploitation began in the early 1970s and due to oil production, compactions of reservoir layers were observed since 1985; they implied seabed subsidence. Consequently, offshore stations were endangered and expensive lifting operations were required. The first explanation of subsidence related the compaction to the pore pressure decrease. The solution was the injection of gas and water into the oilfield in order to repressurize the reservoir. But the

water flooding induced additional subsidence. These compactions increased the oil recovery (positive aspect) but required new set of platforms (negative aspect). Better understanding of this phenomenon is important for maximizing the positive aspects and minimizing the negative ones.

Some authors explain the compaction by the capillary pressure defined by the interface tensions between oil and water. Evidence of capillary pressure effects in geomechanics has been first investigated in fine-grained soils (see Reference [3] for example). More recently, tests were performed on chalk samples saturated by oil and water [1]. In the frames of unsaturated soil mechanics, different authors [3,4] developed constitutive elasto-plastic models with the air–water suction taken as an independent model variable.

Experiments performed on chalk samples have shown two plastic mechanisms: the pore collapse and the frictional failure. The pore collapse could be caused by the breakdown of physico-chemical bonds between the grains inducing some grain-to-grain slip [5], leading to a contractant behaviour (decrease in porosity). This plastic mode appears for large mean stresses and low shear stresses (for example during oedometer test). The frictional failure corresponds to a plastic distortion inducing an increase of porosity. This plastic mechanism appears for high shear stresses (for example during triaxial test). In most models, the two mechanisms are assumed to be independent [6], and two yield surfaces are defined [6,7]. More recently, some authors develop constitutive laws with capillary pressure effects: in the Papamichos [8,9] model, the elastic parameters and the yield surface are suction dependent; in the models developed by Piau and co-workers [10–12], Homand and Shoa [13] and Plischke [14], the collapse behaviour is described by assuming a stress jump (additional stress) between the oil-saturated state and the water-saturated one.

This paper presents a constitutive model developed in the Pasachalk European project. It is a cap-type plasticity model coupled with the Barcelona one [3] for taking the suction effect into account. The creep behaviour of chalk will be not considered in the model. Experimental results obtained in the project will be used to determine the parameters and to validate the model assumptions made in the simulations.

2. EXPERIMENTAL EVIDENCES AND PARAMETERS DETERMINATION

In the Pasachalk project, all tests were performed on an outcrop chalk from Upper Campanian age, called 'Lixhe chalk' which is sampled in the CBR Company quarry near Liège (Belgium). Previous tests showed that its mechanical behaviour is close to that of reservoir chalks [15–17].

Two first series of experiments on chalk samples have been performed along various stress and suction paths: suction-controlled oedometer tests and triaxial tests with chalk samples saturated either by water or by a specific oil called Soltrol 170^{TM} (kerosene).

2.1. Triaxial test

In the outcrop, the chalk was initially water saturated. In order to obtain oil-saturated sample, chalk plug was oven-dried during 48 h (or until constant weight) at 105°C, and saturated under vacuum with oil. The sample was then put in the triaxial cell and was submitted to oil flow corresponding to 3 pore-volumes in order to obtain the maximum possible oil saturation. However, some water menisci, that cannot be removed by oil flooding, could remain in the sample.

Tests were performed under drained conditions at constant loading rate (10^{-3} MPa/s). The stress path was the following: an isotropic loading was followed by an isotropic unloading, and afterwards, shear stress $q = (\sigma_1 - \sigma_3)$ was applied either under constant cell pressure or constant effective mean stress $p' = (\sigma'1 + 2\sigma'3)/3$.

It is observed that the shear strength depends on the saturating fluids: oil-saturated chalk is stiffer and stronger than water-saturated one. Moreover, the transition between 'oil-like' and 'water-like' behaviour is very sharp and appears for water saturation around 1–2%. In general, two types of failures are observed: the pore collapse that engenders plastic volumetric deformations, and the friction failure that corresponds to a brittle rupture. In the both cases, the pre-failure behaviour is quite elastic, therefore, the failure state can be considered also as yield state. Using this plastic criterion, the yield curves of the chalk saturated by water or by oil can be determined, as shown in Figures 1 and 2. One can observe in these two figures that (1) there is a isotropic stress hardening phenomenon for the chalk, especially for high p' values; (2) the brittle
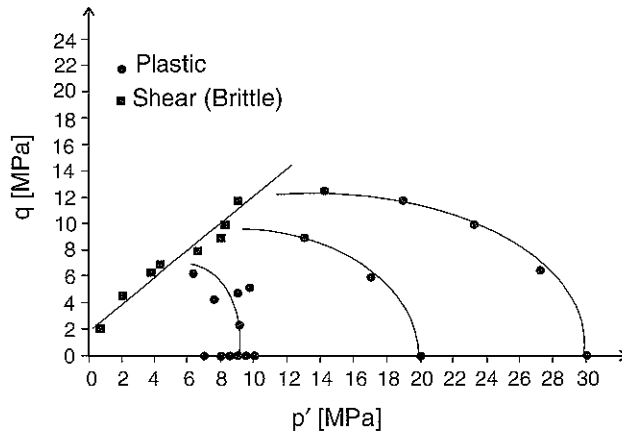

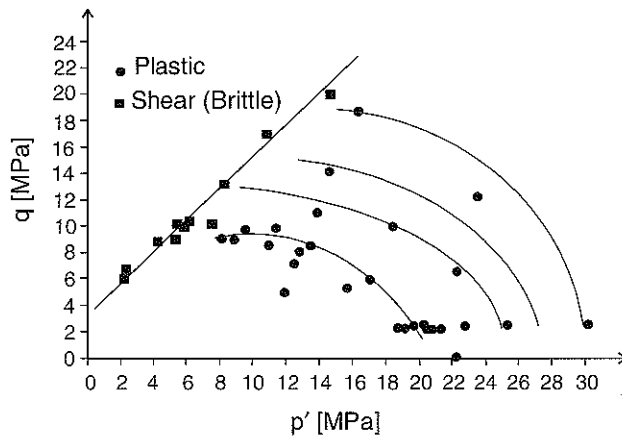Figure 1. Yield curves of water-saturated chalk.

Figure 2. Yield curve of oil-saturated chalk.

rupture is not associated to any hardening phenomenon: the friction yield curve seems to be independent of the cell pressure; (3) the frictional angle does not depend on the saturating fluids: the slope of the friction yield curve is the same for the two types of samples; and (4) the oil-saturated chalk has a bigger elastic domain at a given consolidation stress, evidencing an 'oil' (or suction) hardening phenomenon.

2.2. Oedometer tests

Oedometer tests were performed under different controlled suctions using the osmotic method. This method was used successfully for the case of unsaturated soils [18,19] and it was specially adapted for chalk saturated by oil and water. All tests were carried out using a triaxial press in order to have constant compression rate, which is necessary for the suction control.

Typical results are shown in Figure 3(d). It is observed that the pre-consolidation pressure p_0 increases with the suction increase. The elastic parameter κ corresponding to the small slope and the plastic parameter λ corresponding to large slope seem to be independent on suction. Figure 3(a) and 3(b) present the obtained κ and λ values as a function of suction. Big data scattering makes difficult to deduce any functional dependence. For modelling, κ is taken constant and λ is decreasing function of suction. The pre-consolidation pressure increase with suction is shown in Figure 3(c), which defines the loading collapse (LC) curve of the Barcelona model.

During some tests (Figure 3(d)), the loading process was stopped in order to perform a water flooding and to quantify the induced stress–strain modifications of the chalk sample. It can be
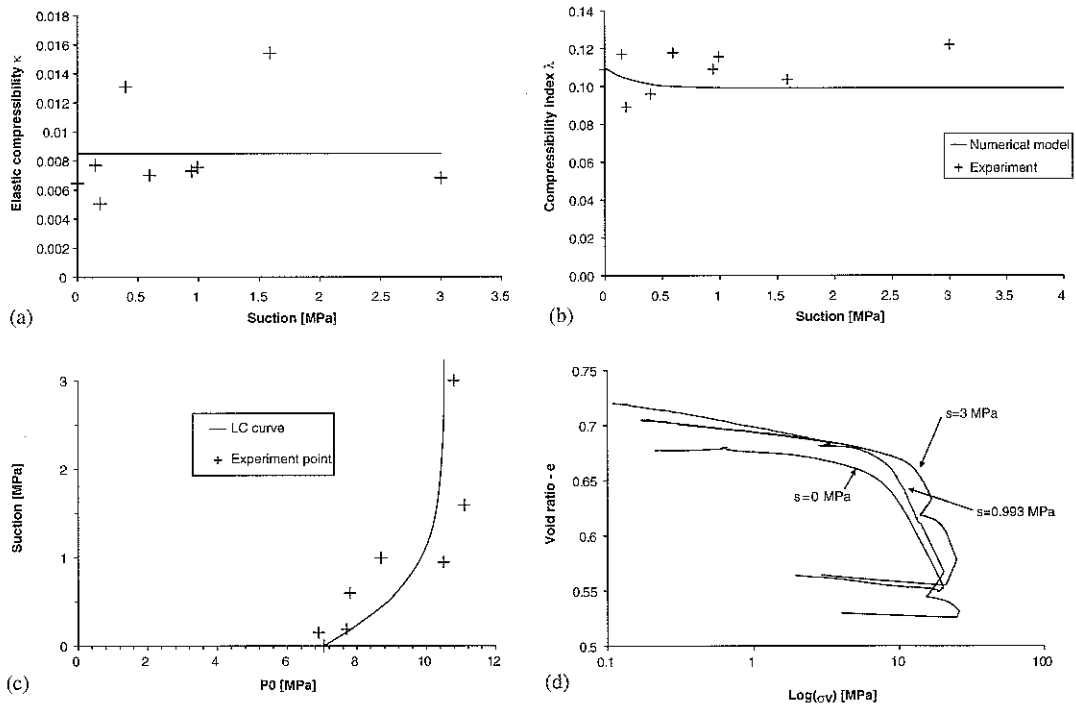

Figure 3. Suction-controlled oedometer tests.

observed that water injection leads to a significant compaction (decreasing void ratio), whilst the associated decrease in the vertical stress (relaxation) is due to the standstill of loading stage on triaxial press. It is worth noting that during subsequent loading after water flooding, all the samples behave as an overconsolidated chalk, and the slope of the compressibility curve reaches the continuity of the initial virgin compressibility slope.

3. CONSTITUTIVE LAW

Based on the experimental results, in most of constitutive models two plastic mechanisms are considered: pore collapse and frictional failure, with two independent yield surfaces [6,20]. In this case, special care has to be taken for the intersection of the yield surfaces, which is an apex that involves numerical difficulties. However, models using only one yield surface have also been developed [8,9]. The expression of these constitutive laws is more complex but including no apex. Difficulties can appear when defining the hardening law, because the two basic physical mechanisms are necessarily coupled. Another solution for apex problems is the use of an additional surface to join the two principal yield surfaces, in order to ensure a continuous slope. The apex is avoided, with a total independence between the two mechanisms. In this paper, the first approach is used and two different yield surfaces are defined.

In order to account for suction effects, it is necessary to consider the evolution of oil and water pressures. It can be done by considering in the model the multi-phase flow.

3.1. Mechanical model

The two evidenced plastic mechanisms are modelled by two yield surfaces combined within a cap model: the modified cam-clay model is used for pore collapse whereas an internal friction model for friction failure. Considering that the chalk strength under extension can be overestimated using an internal friction model, a third yield surface is adopted to limit traction stresses.

Obviously, the so-defined yield curve is not continuously derivable at the intersections, leading to numerical difficulties. However, recent publications provided an elegant way to solve this problem [21].

As far as the suction effect is concerned, the model adopts the approach developed in the Barcelona model [3] where the suction is considered as an independent variable. Suction modifies yield surfaces and suction variations provide reversible and irreversible deformations.

3.1.1. General formulation. The general elastoplastic relations are formulated in rate form. The strain rate $\dot{\epsilon}_{ij}$ is composed of a mechanical part $\dot{\epsilon}_{ij}^{\mathrm{m}}$ and of a suction one $\dot{\epsilon}_{ij}^{\mathrm{s}}$. Each contribution is partitioned in an elastic ($\dot{\epsilon}_{ij}^{\mathrm{m,e}}$ or $\dot{\epsilon}_{ij}^{\mathrm{s,e}}$) and a plastic component ($\dot{\epsilon}_{ij}^{\mathrm{m,p}}$ or $\dot{\epsilon}_{ij}^{\mathrm{s,p}}$):

$$\dot{\epsilon}_{ij} = \dot{\epsilon}_{ij}^{\mathrm{m}} + \dot{\epsilon}_{ij}^{\mathrm{s}}$$
$$= \dot{\epsilon}_{ij}^{\mathrm{m,e}} + \dot{\epsilon}_{ij}^{\mathrm{s,e}} + \dot{\epsilon}_{ij}^{\mathrm{m,p}} + \dot{\epsilon}_{ij}^{\mathrm{s,p}} \tag{1}$$

The mechanical elastic part is related to the stress rate $\dot{\sigma}_{kl}$ through Hooke's law:

$$\dot{\sigma}_{kl} = C_{klij}^{\mathrm{e}} \dot{\epsilon}_{ij}^{\mathrm{m,e}} \tag{2}$$

where the compliance elastic tensor is defined by

$$C^{\mathrm{e}}_{klij} = \frac{E}{1+v}\delta_{ik}\delta_{jl} + \frac{Ev}{(1+v)(1-2v)}\delta_{ij}\delta_{kl} \qquad (3)$$

with the Young modulus E and the Poisson coefficient v.

The elastic deformations induced by suction are given by the following relation which links the strain rate to the suction rate:

$$\dot{\epsilon}^{\mathrm{s,e}}_{ij} = \frac{\kappa_s}{(1+e)}\frac{\dot{s}}{(s+p_{\mathrm{at}})}\delta_{ij} = h^{\mathrm{e}}_{ij}\dot{s} \qquad (4)$$

where e is the void ratio, p_{at} is the atmospheric pressure and κ_s is the elastic coefficient defined in Barcelona model.

The suction is by definition equal to the difference of the oil pressure and water pressure.

For the frictional plastic part, a general framework of non-associated plasticity is adopted in order to limit dilatancy. In that case, the plastic flow rate is derived from a plastic potential g_α:

$$\dot{\epsilon}^{\mathrm{m,p}}_{ij} = \dot{\lambda}^{\mathrm{p}}\frac{\partial g_\alpha}{\partial \sigma_{ij}} \qquad (5)$$

where $\dot{\lambda}^{\mathrm{p}}$ is a scalar multiplicator and g_α is the plastic potential related to the plastic mechanism α.

The other yield surfaces are written in an associated plasticity ($f_\alpha \equiv g_\alpha$).

Irreversible deformations are induced when the suction becomes higher than a suction level s_0. The plastic strain is linked to suction rate with the following relation:

$$\dot{\epsilon}^{\mathrm{s,p}}_{ij} = \frac{\lambda_s - \kappa_s}{(1+e)}\frac{\dot{s}}{(s+p_{\mathrm{at}})}\delta_{ij} = h^{\mathrm{p}}_{ij}\dot{s} \qquad (6)$$

where λ_s is the plastic coefficient defined in Barcelona model.

Equations (1) and (2) can be rewritten as

$$\dot{\epsilon}_{ij} = \dot{\epsilon}^{\mathrm{m,e}}_{ij} + \dot{\epsilon}^{\mathrm{s,e}}_{ij} + \dot{\epsilon}^{\mathrm{m,p}}_{ij} + \dot{\epsilon}^{\mathrm{s,p}}_{ij}$$

$$= C^{\mathrm{e}-1}_{klij}\dot{\sigma}_{kl} + h^{\mathrm{e}}_{ij}\dot{s} + \dot{\lambda}^{\mathrm{p}}\frac{\partial g_\alpha}{\partial \sigma_{ij}} + h^{\mathrm{p}}_{ij}\dot{s} \qquad (7)$$

$$\dot{\sigma}_{kl} = C^{\mathrm{e}}_{klij}\left(\dot{\epsilon}_{ij} - h^{\mathrm{e}}_{ij}\dot{s} - \dot{\lambda}^{\mathrm{p}}\frac{\partial g_\alpha}{\partial \sigma_{ij}} - h^{\mathrm{p}}_{ij}\dot{s}\right) \qquad (8)$$

Considering a general hardening/softening plastic law depending on the internal variable ζ, the consistency condition related to the yield function f_α can be formulated as

$$\dot{f}_\alpha = \frac{\partial f_\alpha}{\partial \sigma_{ij}}\dot{\sigma}_{ij} + \frac{\partial f_\alpha}{\partial s}\dot{s} + \frac{\partial f_\alpha}{\partial \zeta}\dot{\zeta} = 0 \qquad (9)$$

Substituting (8) into (9), the expression of multiplicator $\dot{\lambda}^{\mathrm{p}}$ can be found and the stress rate can be computed as

$$\dot{\sigma}_{kl} = (C^{\mathrm{e}}_{klij} - C^{\mathrm{p}}_{klij})\dot{\epsilon}_{ij} - M_{kl}\dot{s} \qquad (10)$$

The first term of the right part is the classical expression of an elasto-plastic formulation. The second term is related to the suction.
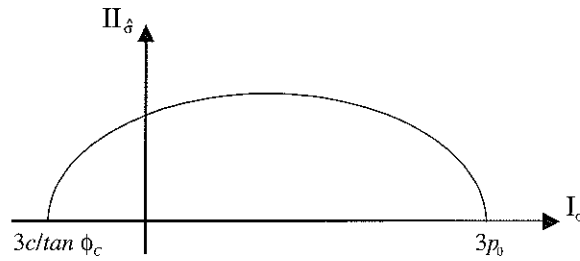
Figure 4. Cam-Clay model—$(I_\sigma, II_{\hat\sigma})$ plane.

3.1.2. Cam-Clay model.

In the modified Cam-Clay model used, the elastic behaviour can be either linear or non-linear. The Cam-Clay yield surface is an ellipse (Figure 4) in the first and second stress invariant plane

$$\left(I_\sigma = \sigma_{ii}, II_{\hat\sigma} = \sqrt{\frac{1}{2}\hat\sigma_{ij}\hat\sigma_{ij}}, \hat\sigma_{ij} = \sigma_{ij} - \frac{I_\sigma}{3}\delta_{ij}\right):$$

$$f_1 \equiv II_{\hat\sigma}^2 + m^2\left(I_\sigma + \frac{3c}{\tan\phi_C}\right)(I_\sigma - 3p_0) = 0 \tag{11}$$

where c is the cohesion, ϕ_C is the friction angle in compression path, p_0 is the pre-consolidation pressure which defines the size of the yield surface and m is a coefficient introduced to take into account the effect of the third stress invariant $III_{\hat\sigma} = \frac{1}{3}\hat\sigma_{ij}\hat\sigma_{jk}\hat\sigma_{ki}$.

The coefficient m is defined by

$$m = a(1 + b\sin 3\beta)^n \tag{12}$$

where

$$\beta = -\frac{1}{3}\sin^{-1}\left(\frac{3\sqrt{3}}{2}\frac{III_{\hat\sigma}}{II_{\hat\sigma}^3}\right) \tag{13}$$

β is the Lode angle which can be derived from the definition of the third stress invariant, and the three parameters a, b and n must verify some convexity conditions [22]. It should be noted that the introduction of β leads to a non-circular surface shape in the shear plan.

The plastic flow is supposed to be associated $f_1 \equiv g_1$. The internal variable is the pre-consolidation pressure p_0, which depends on the volumetric plastic deformations $d\epsilon_v^p$ and has the following kinematic equation:

$$dp_0 = \frac{1 + e}{\lambda - \kappa} p_0 \, d\epsilon_v^p \tag{14}$$

where λ is the compression coefficient and κ is the elastic coefficient. The volumetric plastic deformation rate is given by

$$\dot\epsilon_v^p = \dot\lambda^p \frac{\partial g_1}{\partial\sigma_{ij}}\delta_{ij} \tag{15}$$

Using this relation, either hardening or softening could appear according to the sign of the volumetric plastic deformations (Figure 5). However, in the cap model, the softening zone will not be considered.
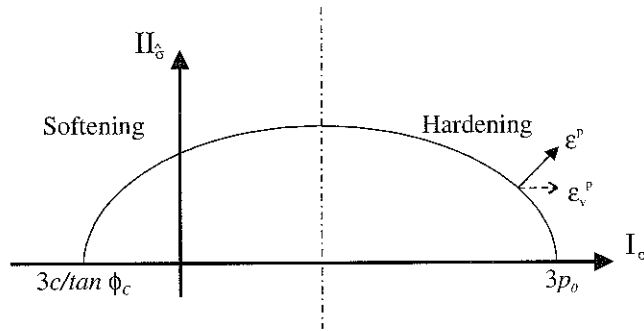
Figure 5. Hardening–softening zones.

3.1.3. Internal friction model. A more sophisticated model can be built from the cone of Drucker–Prager by introducing a dependence on the Lode's angle β, in order to match more closely the Mohr–Coulomb criterion. It consists of a smoothed Mohr–Coulomb plasticity surface. The formulation proposed by Barnichon [23], based on the idea of Van Eekelen [22], is used. It can be written in a very similar way to the criterion of Drucker–Prager:

$$f_2 \equiv \mathrm{II}_{\hat{\sigma}} - m\left(\mathrm{I}_\sigma + \frac{3c}{\tan\phi_C}\right) = 0 \tag{16}$$

A non-associated plasticity is considered here using the dilatancy angle ψ, which depends on the hardening process:

$$g_2 \equiv \mathrm{II}_{\hat{\sigma}} - m'\left(\mathrm{I}_\sigma + \frac{3c}{\tan\phi_C}\right) = 0 \tag{17}$$

where m' has the same definition of coefficient m (12), using dilatancy angle instead of frictional angle.

The internal variables are the frictional angles ϕ_C (for compression paths), ϕ_E (for extension paths) and the cohesion c. The following hardening relations are defined using the plastic equivalent deformations ϵ_{eq}^p:

$$\phi_C = \phi_{C0} + \frac{(\phi_{Cf} - \phi_{C0})\epsilon_{eq}^p}{B_p + \epsilon_{eq}^p}$$

$$\phi_E = \phi_{E0} + \frac{(\phi_{Ef} - \phi_{E0})\epsilon_{eq}^p}{B_p + \epsilon_{eq}^p} \tag{18}$$

$$c = c_0 + \frac{(c_f - c_0)\epsilon_{eq}^p}{B_c + \epsilon_{eq}^p}$$

where subscripts 0 and f mean the initial and the final values, respectively; B_p and B_c are the parameters defining the plastic deformation for which half of the internal variable hardening is achieved. Figure 6 presents the effect of B_p on the hyperbolic hardening relation.

The equivalent strain ϵ_{eq}^p represents the cumulated equivalent plastic strains during time t:

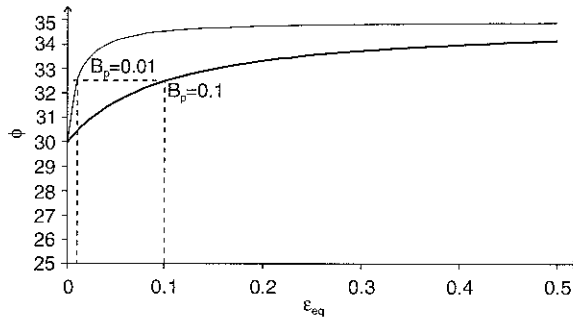$$\epsilon_{eq}^p = \int_0^t \dot{\epsilon}_{eq}^p \, dt \tag{19}$$

Figure 6. Hyperbolic hardening relation for two values of coefficient B_p ($B_p = 0.01$ and $B_p = 0.1$), and with $\phi_0 = 30°$, $\phi_f = 35°$.

where the equivalent strain rate is given by

$$\dot{\epsilon}_{cq}^p = \sqrt{\frac{2}{3}\dot{\epsilon}_{ij}^p\dot{\epsilon}_{ij}^p} = \dot{\lambda}^p\sqrt{\frac{2}{3}\left(\frac{\partial g}{\partial \sigma_{ij}}\frac{\partial g}{\partial \sigma_{ij}} - \frac{1}{3}\frac{\partial g}{\partial \sigma_{kk}}\frac{\partial g}{\partial \sigma_{ll}}\right)} \qquad (20)$$

3.1.4. Traction model. Traction strength defined in the internal friction model (16) depends on both friction angle and cohesion. Experimental evidences [24] show that this model overestimates the traction strength of chalk. To avoid this drawback, a third yield surface is introduced with σ_t as traction limit in terms of mean stress:

$$f_3 \equiv I_\sigma + 3\sigma_t = 0 \qquad (21)$$

Associated plasticity is used for this surface, and no hardening is included.

3.1.5. Suction effect on yield surfaces. As mentioned above, the oil–water suction has an effect on the mechanical behaviour of chalk containing oil and water. Suction changes can induce both elastic and plastic strains. The formulation related to suction is performed as follows:

• The pre-consolidation pressure p_0 increases with suction increase and is described using the LC concept of the Barcelona model:

$$p_0(s) = p_c\left(\frac{p_0^*}{p_c}\right)^{(\lambda(0)-\kappa)/(\lambda(s)-\kappa)} \qquad (22)$$

with

$$\lambda(s) = \lambda(0)[(1-r)\exp(-\beta's) + r] \qquad (23)$$

where p_0^* is the pre-consolidation pressure for $s = 0$, p_c is the reference pressure, $\lambda(0)$ is the compression coefficient at zero suction, $\lambda(s)$ is the compression coefficient at suction s, r is a parameter representing the maximum stiffness of the chalk, and β' is the parameter controlling the stiffness increase with suction increase.

Figure 7. Yield surfaces in $(I_\sigma, II_{\hat{\sigma}}, s)$ space.

- Cohesion increases with suction according to the relationship:

$$c(s) = c(0) + ks \tag{24}$$

  where k is the material constant and $c(0)$ is the cohesion at saturated state.
- The friction angle is not suction dependent.
- Suction is supposed to have no influence on traction strength σ_t.
- When suction becomes higher than a suction level s_0, irreversible strains are created. A fourth yield surface, the 'suction increase' (SI) curve defined in the Barcelona model, is introduced in our constitutive law:

$$f_4 \equiv s - s_0 = 0 \tag{25}$$

  Figure 7 presents all the yield surfaces in the space $(I_\sigma, II_{\hat{\sigma}}, s)$.

3.1.6. Numerical integration. The existence of four yield surfaces in the model leads to complex law integration. One has to not only determine which plastic mechanism is active, but also manage the case where two surfaces are active. This case occurs at the intersection of two surfaces: the apex regime is a combination of two mechanisms.

Figure 8 presents the three first yield curves with different possible plastic regimes:

- Cam-Clay mechanism active: IYIELD = 1
- Internal friction mechanism active: IYIELD = 2
- Traction limitation mechanism active: IYIELD = 3
- Both internal friction and Cam-Clay mechanisms active: IYIELD = 4
- Both internal friction and traction limitation mechanisms active: IYIELD = 5.

The SI curve is not taken into account here for sake of simplicity. Otherwise, the procedure would be exactly the same.
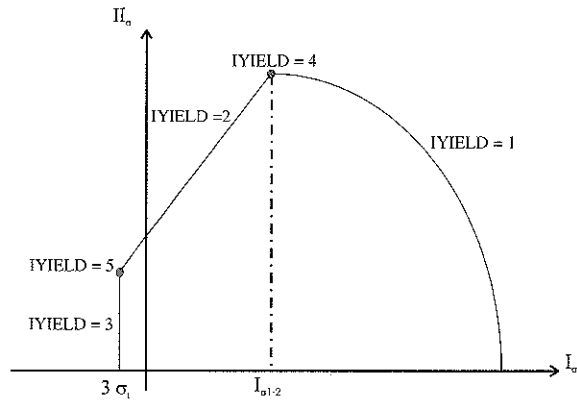
Figure 8. Cap model, combination of three yield surfaces.

Integration over time of the general rate constitutive elasto-plastic relation (10) leads to the incremental form:

$$\Delta\sigma_{ij} = (C^{e}_{ijkl} - C^{p}_{ijkl})\Delta\epsilon_{kl} - M_{kl}\Delta s \qquad (26)$$

The method used here is commonly based on the operator-split methodology [25], which consists in computing an elastic predictor/plastic corrector. Once the elastic predictor is computed, one can determine the active plastic regime. This is important when the stress state is close to an apex. It must be mentioned that the notion of proximity is relative and arbitrary. In this model, the following routine has been chosen (see Figure 8):

1. Computation of the mean stress at the intersection of the internal friction model and Cam-Clay model:

$$I_{\sigma,1-2} = \left(\frac{3c}{\text{tg}\,\phi} - 3p_0\right)\Big/ 2 \qquad (27)$$

2. If $I_\sigma > I_{\sigma,1-2} + I_{\sigma,1-2}/2$, only the Cam-Clay model could be active (IYIELD = 1).
3. If $I_{\sigma,1-2} - I_{\sigma,1-2}/2 < I_\sigma < I_{\sigma,1-2} + I_{\sigma,1-2}/2$, both Cam-Clay model and internal friction model could be active (IYIELD = 4).
4. If $3\sigma_t < I_\sigma < I_{\sigma,1-2} - I_{\sigma,1-2}/2$, only the internal friction model could be active (IYIELD = 2).
5. If $I_\sigma < 3\sigma_t$, both internal friction model and traction limitation model could be active (IYIELD = 5).

Hughes and Simo [21] proposed a technique for integrating the law in an apex regime in accordance with which for IYIELD = 4, the following consistency conditions must be verified:

$$
\begin{aligned}
f_1 &= 0 \quad \text{and} \quad f_2 = 0 \\
\dot{f}_1 &= 0 \quad \text{and} \quad \dot{f}_2 = 0
\end{aligned}
\qquad (28)
$$

with f_1 and f_2 being the yield functions related to the plastic mechanisms 1 and 2, respectively.

The plastic strain is a sum of the plastic strains due to the mechanisms 1 and 2:

$$\dot{\epsilon}_{ij}^{p} = \dot{\epsilon}_{ij}^{p,1} + \dot{\epsilon}_{ij}^{p,2} = \dot{\lambda}^{p,1}\frac{\partial g_1}{\partial \sigma_{ij}} + \dot{\lambda}^{p,2}\frac{\partial g_2}{\partial \sigma_{ij}} \tag{29}$$

where g_1 and g_2 are the plastic potentials associated, respectively, to the plastic mechanisms 1 and 2.

Considering that yield surfaces (f_α, $\alpha = 1, 2$) are only function of the stress state (σ_{ij}), suction s and hardening variables (ζ^α), the Taylor's series expansions for consistency conditions (28) are given as

$$f_\alpha(\sigma_{ij} + \Delta\sigma_{ij}^{p}, s + \Delta s, \zeta^\alpha + \Delta\zeta^\alpha) = f_\alpha(\sigma_{ij}, s, \zeta^\alpha) + \frac{\partial f_\alpha}{\partial \sigma_{ij}}\Delta\sigma_{ij}^{p} + \frac{\partial f_\alpha}{\partial s}\Delta s$$

$$+\frac{\partial f_\alpha}{\partial \zeta^\alpha}\Delta\zeta^\alpha, \quad \alpha = 1, 2 \tag{30}$$

with

$$\Delta\sigma_{ij}^{p} = -C_{ijkl}^{e}\Delta(\epsilon_{kl}^{p,1} + \epsilon_{kl}^{p,2}) \tag{31}$$

$$\Delta\zeta^\alpha = \frac{d\zeta^\alpha}{d\epsilon^{p,\alpha}}\Delta\epsilon^{p,\alpha} \tag{32}$$

Knowing that Equations (15) and (20) can be expressed in a more general form:

$$\Delta\epsilon^{p,\alpha} = \dot{\lambda}^{p}\text{Val}^\alpha \tag{33}$$

and using Equations (29), (31) and (32), Equation (30) can be rewritten as

$$f_\alpha = f_\alpha(\sigma_{ij}, s, \zeta^\alpha) - \frac{\partial f_\alpha}{\partial \sigma_{ij}}C_{ijkl}^{e}\left(\sum_{n=1}^{2}\Delta\lambda^{p,n}\frac{\partial g_n}{\partial \sigma_{kl}}\right) + \frac{\partial f_\alpha}{\partial s}\Delta s$$

$$+ \text{Val}^\alpha\frac{\partial f_\alpha}{\partial \zeta^\alpha}\frac{d\zeta^\alpha}{d\epsilon^{p,\alpha}}\Delta\lambda^{p,\alpha} \tag{34}$$

Knowing that in the plastic regime $f = 0$, the previous relation gives an incremental consistency equation for each mechanisms.

$$f_1(\sigma_{ij}, \zeta^1) - \frac{\partial f_1}{\partial \sigma_{ij}}C_{ijkl}^{e}\left(\Delta\lambda^{p,1}\frac{\partial g_1}{\partial \sigma_{kl}} + \Delta\lambda^{p,2}\frac{\partial g_2}{\partial \sigma_{kl}}\right) + \frac{\partial f_1}{\partial s}\Delta s$$

$$+ \text{Val}^1\frac{\partial f_1}{\partial \zeta^1}\frac{d\zeta^1}{d\epsilon^{p,1}}\Delta\lambda^{p,1} = 0$$

$$f_2(\sigma_{ij}, \zeta^2) - \frac{\partial f_2}{\partial \sigma_{ij}}C_{ijkl}^{e}\left(\Delta\lambda^{p,1}\frac{\partial g_1}{\partial \sigma_{kl}} + \Delta\lambda^{p,2}\frac{\partial g_2}{\partial \sigma_{kl}}\right) + \frac{\partial f_2}{\partial s}\Delta s$$

$$+ \text{Val}^2\frac{\partial f_2}{\partial \zeta^2}\frac{d\zeta^2}{d\epsilon^{p,2}}\Delta\lambda^{p,2} = 0 \tag{35}$$

The system of equations provide the value of the two plastic multiplicators, $\Delta\lambda^{p,1}$ and $\Delta\lambda^{p,2}$. When both values are positive, the two mechanisms are activated simultaneously, however, if one multiplicator is negative, the corresponding mechanism must not be activated, and the computation is reiterated only with the other yield surface.

3.2. Diffusion model

Unsaturated flow formulation is used here, which is based on works in relation with the problem of nuclear waste disposal [26–28]. For each fluid (water and oil), balance equations are written by considering the variation of fluid storage equal to the difference between the input and output flows of an elementary volume. The unsaturated flow model derives from equations of saturated conditions. The permeability and the storage law have to be modified in partial saturation conditions [29]. A generalized Darcy's law defines the fluid motion [30]. Numerous couplings existing between mechanics and flows are considered.

3.2.1. Water. The generalized Darcy's law for multiphase porous medium gives liquid water velocity:

$$ \underline{f}_{\mathrm{w}} = -\frac{k_{\mathrm{r,w}} k_{\mathrm{int}}^{\mathrm{sat}}}{\mu_{\mathrm{w}}} [\underline{\mathrm{grad}}(p_{\mathrm{w}}) + g \rho_{\mathrm{w}} \underline{\mathrm{grad}}(y)] \tag{36} $$

where $\underline{f}_{\mathrm{w}}$ is the water macroscopic velocity, ρ_{w} is the water density, p_{w} is the liquid water pressure, y is the vertical upward directed co-ordinate, g is the gravity acceleration, μ_{w} is the dynamic viscosity of the liquid water, $k_{\mathrm{int}}^{\mathrm{sat}}$ is the intrinsic permeability of the medium and $k_{\mathrm{r,w}}$ is the water relative permeability which varies with respect to the saturation degree.

The balance equation includes the variation of water storage and the divergence of water flows:

$$ \frac{\partial}{\partial t} f_{\mathrm{w}}^* + \mathrm{div}(\rho_{\mathrm{w}} \underline{f}_{\mathrm{w}}) = 0 \tag{37} $$

where t is the time and f_{w}^* is the water storage:

$$ f_{\mathrm{w}}^* = \rho_{\mathrm{w}} n S_{\mathrm{r,w}} \tag{38} $$

with n being the porosity and $S_{\mathrm{r,w}}$ the water saturation degree.

The water density is dependent on water pressure according to

$$ \rho_{\mathrm{w}} = \rho_{\mathrm{w,0}} \left(1 + \frac{p_{\mathrm{w}} - p_{\mathrm{w,0}}}{\chi_{\mathrm{w}}} \right) \tag{39} $$

where $\rho_{\mathrm{w,0}}$ is the water density at reference pressure $p_{\mathrm{w,0}}$, ρ_{w} is the density at pressure p_{w} and χ_{w} is the water compressibility.

3.2.2. Oil. Considering the generalized Darcy's law for multiphase porous medium, oil velocity is given by

$$ \underline{f}_{\mathrm{o}} = -\frac{k_{\mathrm{r,o}} k_{\mathrm{int}}^{\mathrm{sat}}}{\mu_{\mathrm{o}}} [\underline{\mathrm{grad}}(p_{\mathrm{o}}) + g \rho_{\mathrm{o}} \underline{\mathrm{grad}}(y)] \tag{40} $$

where $\underline{f}_{\mathrm{o}}$ is the oil macroscopic velocity, ρ_{o} is the oil density, p_{o} is the oil pressure, μ_{o} is the dynamic viscosity of oil and $k_{\mathrm{r,o}}$ is the oil relative permeability which depends on the oil saturation degree $S_{\mathrm{r,o}} = 1 - S_{\mathrm{r,w}}$.

The oil balance equation is given by the relation:

$$ \frac{\partial}{\partial t} f_{\mathrm{o}}^* + \mathrm{div}(\rho_{\mathrm{o}} \underline{f}_{\mathrm{o}}) = 0 \tag{41} $$

and the oil storage is defined by

$$f_o^* = \rho_o n S_{r,o} \qquad (42)$$

The oil density is depending on oil pressure according to a relationship similar to Equation (39).

4. DETERMINATION OF PARAMETERS

The constitutive model needs the determination of the mechanical and hydraulic properties. Most of the parameters are defined using the tests performed during the project. For the mechanical parameters identification, triaxial and oedometric tests data are used.

4.1. Triaxial test on saturated (by oil or water) samples

The tests were carried out on chalk samples saturated by two fluids: water and Soltrol^{TM} (normalized oil). Assuming a linear elasticity, the elastic parameters can be determined using experimental results presented in the plane (ε_v, p') and $(\varepsilon_{eq}, II_{\hat{\sigma}})$ (Figure 9). According to the model, the elastic part of the stress path is linear in these planes and the slopes are, respectively, K and $3G$ where $K = E/3(1 - 2v)$ is the bulk modulus and $G = E/2(1 + v)$ is the shear modulus. Figure 9 shows that this assumed linearity is well verified. Table I gives the obtained elastic parameters.

Triaxial tests data are used to determine the pre-consolidation pressure p_0 corresponding to the point of slope change in the plane (ε_v, p') (Figure 9), and the failure parameters c and ϕ. Table II gives the mean values of these parameters.

Figure 10 shows the comparison between experimental results and numerical modelling for triaxial tests on water- and oil-saturated samples. The experimental path of Figure 10 shows a mechanical hysteresis, which is not captured by the model. However, the qualitative agreement shows that the constitutive law permits to describe the mechanical behaviour of unsaturated chalk.

4.2. Oedometer tests under unsaturated conditions

Oedometer tests were performed for different suction values. Using the experimental results, the parameters κ, λ and p_0 can be determined in a manner as follows (Figure 11).

Assuming a non-linear elasticity, the three parameters are determined as a function of the suction (Figure 3). In the Barcelona model [3], the κ coefficient is not suction dependent; as shown in Figure 3(a), the measured values of this parameter seem highly scattered.

Important scattering is also observed for the λ values in Figure 3(b). A relationship is assumed with respect to Equation (23). It should be noticed that according to the expression of LC curve (22) the λ values has important effects on the shape of LC.

The function $\lambda(s)$ and the reference pressure p_c were chosen in a manner that the LC curve fits well with the experimental results (Figure 3(c)). The determined parameters are presented in Table III.

In Figure 12, the experimental results are compared to the numerical simulations at two suction values (0 and 3 MPa). At 3 MPa of suction, a water flooding was carried out (together with a relaxation phenomenon) during the plastic phase. This flooding was not modelled. A qualitative good agreement between experimental and numerical results is obtained.
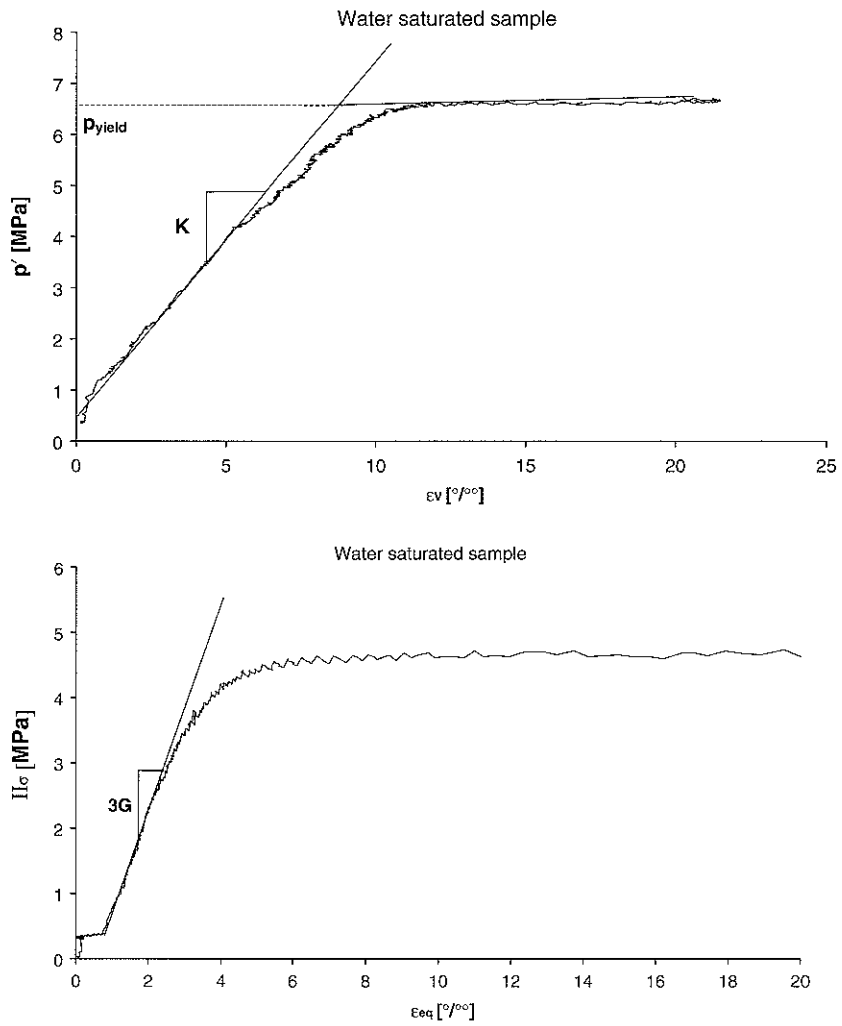
Figure 9. Determination of the elastic moduli and the yield points.

Table I. Elastic parameters.

Fluid	Water	Soltrol[TM]
E (MPa)	1366	1483
v	0.20	0.18

Table II. Strength parameters.

Fluid	Water	Soltrol[TM]
$\varphi(^\circ)$	25	25
c (MPa)	1.5	2.0
p_0 (MPa)	12	18
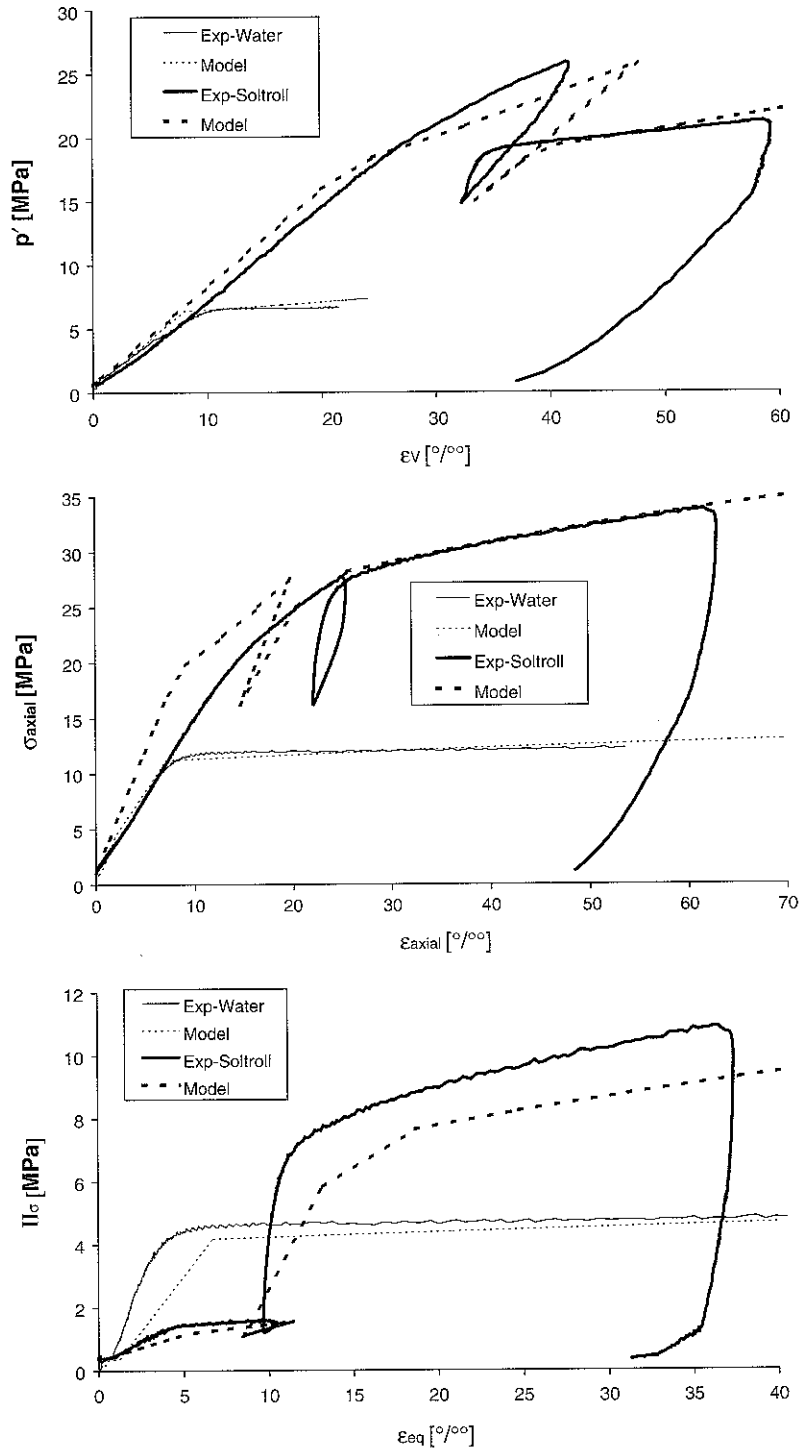
Figure 10. Comparison between triaxial experiments and numerical simulations.
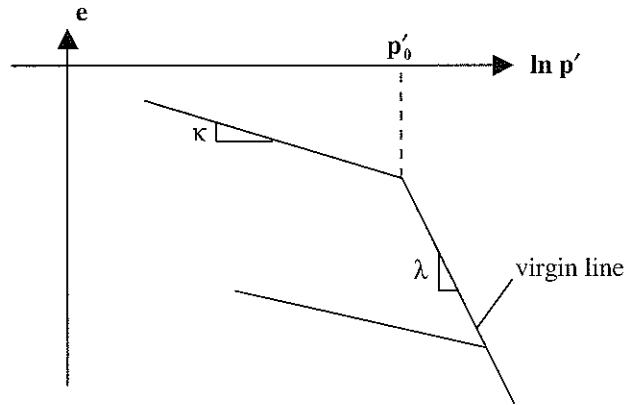
Figure 11. Determination of parameters κ, λ and p_0 using oedometer test results.

Table III. Parameters determined using oedometer tests.

$\lambda(0)$	r	β (1/MPa)	p_c (MPa)	κ	p_0 (MPa)
0.11	0.8	2.00	1.65	0.0085	7.05
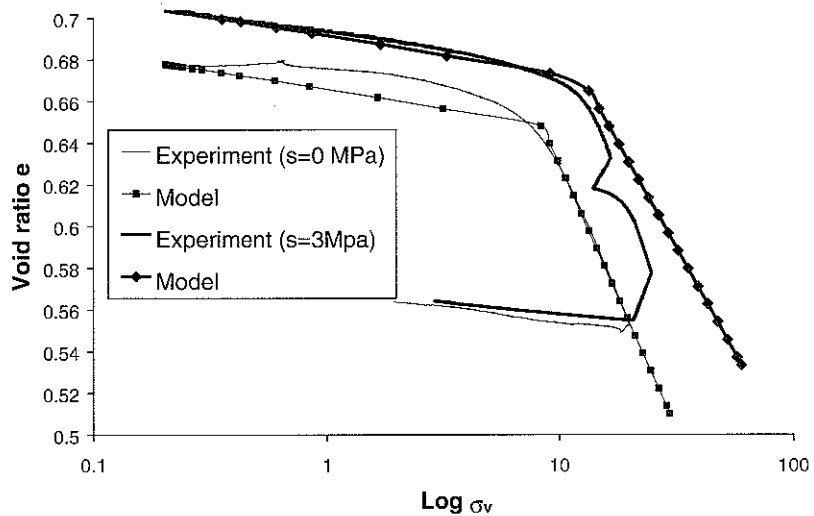
Figure 12. Suction-controlled oedometer tests.

4.3. Hydraulic parameters and fluids properties

Suction affects deeply the mechanical behaviour of chalk. Thus, the fluid motion in the chalk is very important to be considered through the hydraulic properties of the chalk and the properties of the pore fluids (water and Soltrol[TM]).

4.3.1. Fluids properties. The main properties of the different fluids are the volumetric mass, the compressibility and the dynamic viscosity. The following values are considered (Table IV).

The volumetric mass and the dynamic viscosity of Soltrol™ are those defined by the producer (PHILLIPS Chemical Company) for Soltrol 170™. The value of the oil compressibility is unknown but has been taken by default the same as for water.

4.3.2. Hydraulic properties of chalk. The chalk hydraulic characteristics involve the porosity, the intrinsic and the relative permeability and the retention curve. The chalk porosity depends on chalk origin and its geological history. A mean value of 40% is assumed. The intrinsic permeability k_{int}^{sat} can be calculated from permeability coefficient K in m/s using the following relation:

$$k_{int}^{sat} = \frac{K\mu}{\rho g} \tag{43}$$

For Lixhe chalk, in saturated conditions, the intrinsic permeability k_{int}^{sat} is assumed to be equal to 1.688×10^{-15} m^2.

Chalk permeability to the different fluids depends on the degree of saturation. The water permeability $k_{int,wat}^{unsat}$ and the oil permeability $k_{int,oil}^{unsat}$ are calculated by

$$k_{int,wat}^{unsat} = k_{r,water}\, k_{int}^{sat}, \quad k_{int,oil}^{unsat} = k_{r,oil}\, k_{int}^{sat} \tag{44}$$

with $k_{r,water}$ and $k_{r,oil}$ as water and oil relative permeability, respectively.

Generally in unsaturated soils mechanics, the relative permeability is supposed to be a function of the saturation degree. Ebeltoft *et al.* [31] worked on three chalks (A, B and C) and obtained an increase in permeability with the saturation degree (Figures 13 and 14), which is in agreement with common results obtained for unsaturated soils. These experiment data are fitted
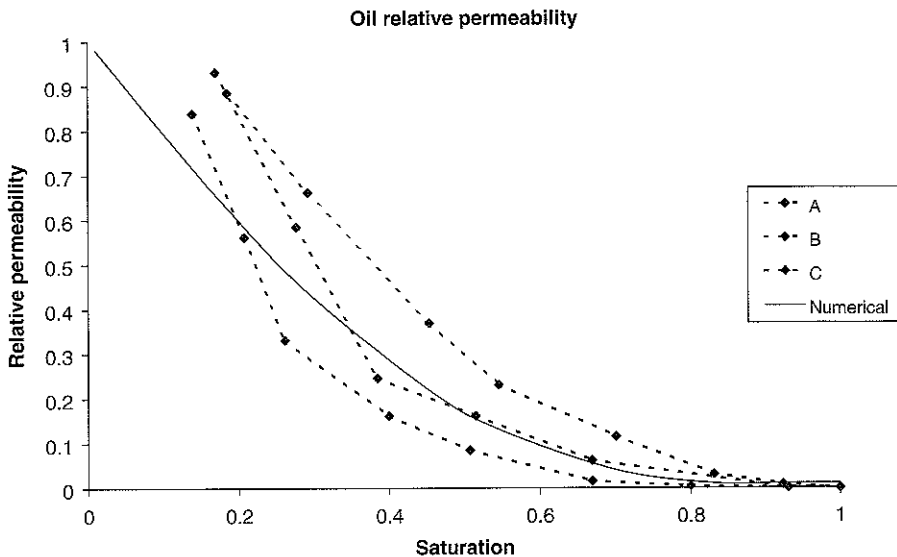

Figure 13. Oil relative permeability (A,B,C curves: experiment [31]).

Table IV. Fluids properties.

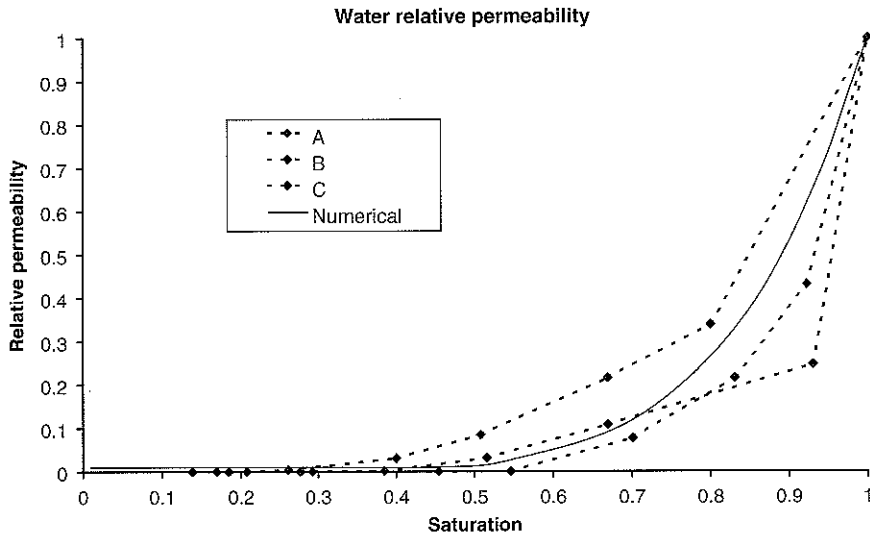| Fluid	Water	Soltrol^{TM}
Volumetric mass ρ_0 at atmospheric pressure p_0	1000 kg/m^3	782.551 kg/m^3
Compressibility χ	3×10^9 Pa	3×10^9 Pa
Dynamic viscosity μ at $T = 20°$C	1.009×10^{-3} Pa s	3.0085×10^{-3} Pa s

Figure 14. Water relative permeability (A, B, C curves: experiment [31]).

using the following expressions [32]:

$$k_{\mathrm{rel,oil}} = (1 - S_{\mathrm{e}})^2 (1 - S_{\mathrm{e}}^{5/3}) \tag{45}$$

$$k_{\mathrm{rel,water}} = \frac{(S_{\mathrm{r,w}} - S_{\mathrm{res}})^6}{(S_{\mathrm{r,field}} - S_{\mathrm{res}})^6} \tag{46}$$

where $S_{\mathrm{e}} = (S_{\mathrm{rw}} - S_{\mathrm{res}})/(S_{\mathrm{r,field}} - S_{\mathrm{res}})$ is the effective saturation, S_{res} is the residual saturation and $S_{\mathrm{r,field}}$ is the field saturation.

The experimental curve fitting (see Figures 13 and 14) gives $S_{\mathrm{res}} = 0.01$; $S_{\mathrm{r,field}} = 1$.

The porosimetric curve of Lixhe chalk (Figure 15) provides us fitting the retention curve. The following expression is proposed:

$$S_{\mathrm{r,w}} = \frac{\mathrm{CSR3}}{\pi} \arctan\left(-\frac{s + \mathrm{CSR2}}{\mathrm{CSR1}}\right) + \frac{\mathrm{CSR3}}{2} \tag{47}$$

where CSR1, CSR2, and CSR3 are soil constants with values CSR1 = 100 kPa; CSR2 = −325 kPa and CSR3 = 1.

Retention curves found in the literature [31] (curves A, B and C in Figure 15) are similar to that for Lixhe chalk.
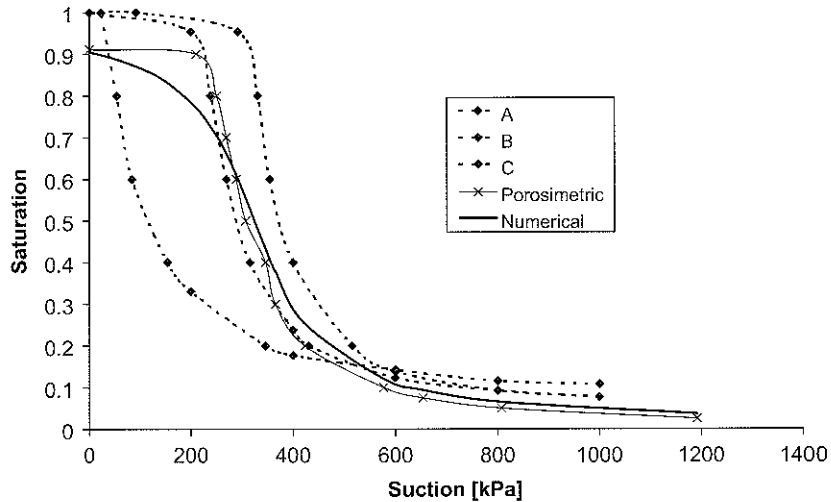
Figure 15. Retention curves of chalk (A, B, C curves [31] and Pasachalk experimental results).

It should be mentioned that all these curves are defined for drying paths. However, in the case of water flooding it involves rather wetting paths. Moreover, during a water-flooding test (see Section 5), water drives out the oil present in the pores but a residual quantity of oil (about 30%) remains in the sample. This corresponds to the well-known hysteresis phenomenon. To match this experimental result, some numerical modifications are necessary, giving rise to the retention curve presented in Figure 16 and defined by the following parameters:

CSR1 = 1.0×10^5 Pa; CSR2 = -9.50×10^4 Pa and CSR3 = 0.75 for wetting path.

Using this curve, 'negative' suctions appear for saturation degree more than 70%. Physically, this negative suction means that a positive water pressure is necessary to increase the water saturation up to 100%. In the mechanical model, the negative suction is not taken into account; if the suction is lower than zero, its effect on the stress state vanishes.

4.4. Discussions

Information about the mechanical behaviour and about the mechanical parameters has been obtained thanks to triaxial tests (including an initial isotropic stress path) and to oedometer tests. However, these two tests are rather different from the point of view of the devices, of the method of loading, of the stress state, of the friction effect on measures, and on the loading rate (involving different creep effects). Therefore, the two approaches of the mechanical parameters may not be fully consistent, and some choices or compromises have to be put.

In the following, we mainly base our model on the triaxial tests, but some data are also given from the oedometer ones. The adopted values are given in the Table V.

In the following section, a water-flooding test will be modelled. During this test, the stress state will not change highly. Therefore, linear as well as non-linear elasticity should give similar results, as the bulk modulus is similar for the two kinds of formulation (Figure 17).
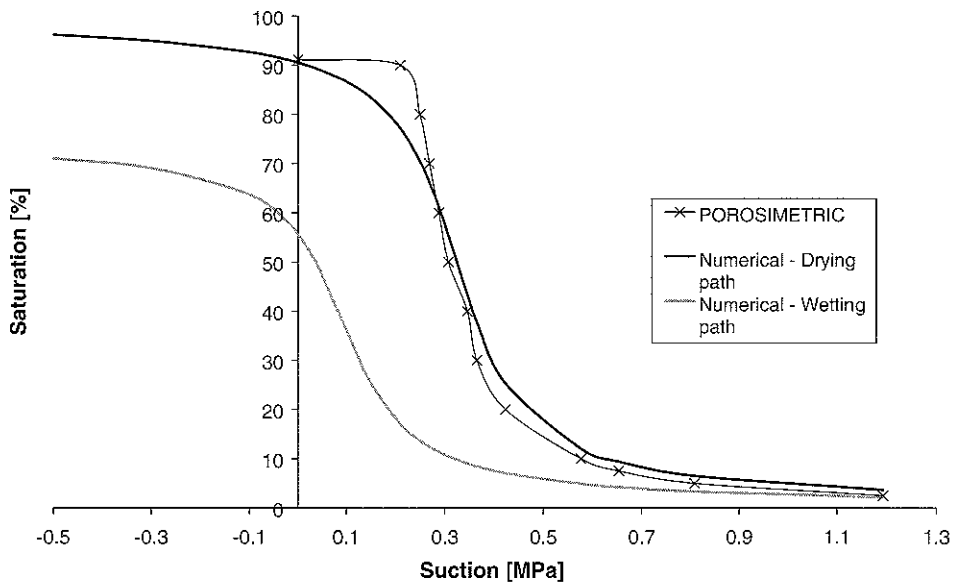
Figure 16. Modified retention curve for wetting path.

Table V. Parameters of the cap model.

	Parameter	Value	Unit	Origin
Non-linear elasticity				
	κ	0.0085	——	Oedometer
	ν	0.2	——	Oedometer
Frictional plastic mechanism				
	ϕ_{water}	25	Degree	Triaxial
	ϕ_{oil}	25	Degree	Triaxial
	c_{water}	15	MPa	Triaxial
	c_{oil}	2.0	MPa	Triaxial
	k	0.167	——	——
Cam-Clay+suction LC				
	$p_{o,water}$	12	MPa	Triaxial-isotropic
	$p_{o,oil}$	18	MPa	Triaxial-isotropic
Hardening rule				
	$\lambda(0)$	0.18	—	Triaxial
	r	0.95	—	Triaxial
	β'	8.0	MPa^{-1}	Triaxial
	p_c	3×10^{-3}	MPa	Triaxial

The initial pre-consolidation threshold (at the initial suction level) is often given by the problem idealization. It is especially the case of the water-flooding test described in the next section.
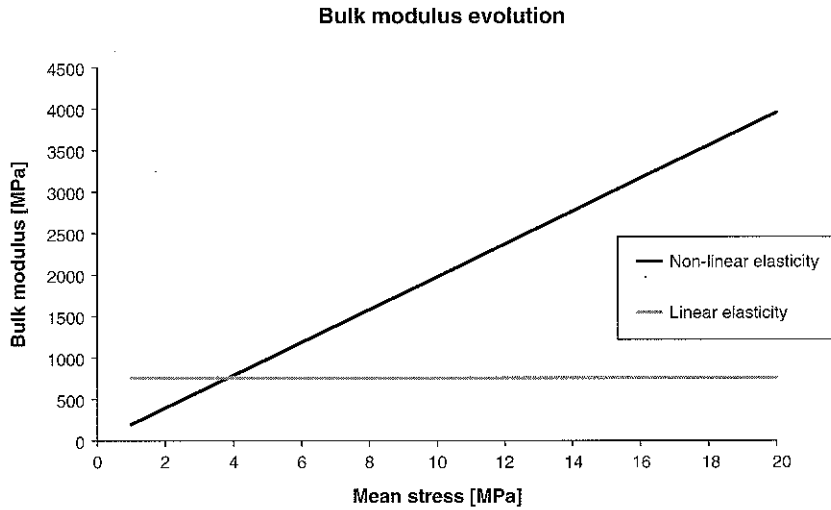
Bulk modulus evolution

Figure 17. Comparison between linear and non-linear elasticity.
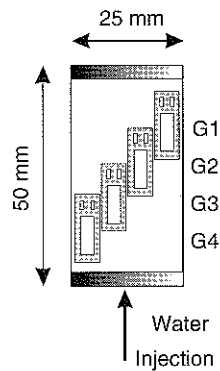

Figure 18. Sketch of the sample for the water-flooding test.

5. WATER-FLOODING TEST MODELLING

The water-flooding test performed on Lixhe chalk initially saturated by Soltrol^{TM} [33] allows to validate the developed model and to complete the set of parameters.

5.1. Description

The sample with an initial porosity $n = 40.55\%$ has a dimension of 25 mm diameter and 50 mm height. Four strain gauges are glued on the sample (located respectively from the injection side at a distance of 4, 12, 22 and 30 mm), which aims to monitoring the evolution of the axial deformation with the water front. In addition, an axial LVDT records the global axial deformation. Figure 18 shows the sample with the four strain gauges G1, G2, G3 and G4.
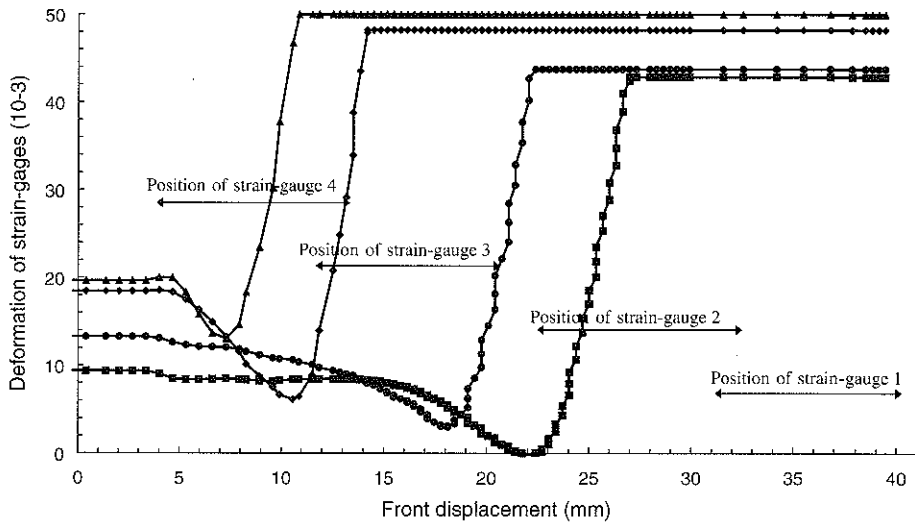
Figure 19. Axial strains during water-flooding test.

The initial stress state is isotropic at a level of 18 MPa, just below the expected pore collapse for 'oil-like' plug. The injection water pressure is equal to 0.9 MPa. Figure 19 shows the strain-gauges response as a function of the 'theoretical' displacement of injection front. The displacement of the injection front was based on the assumption of a piston-like behaviour and of oil saturation behind the front equal to 30% (this value comes from usual results of petrophysical laboratory experiments). Just before the front, a small swelling is measured by the strain gauges but a severe and quasi-instantaneous compaction appears at the water front. The final amplitude of the compaction is around 2–3%.

5.2. Numerical simulations

The modelling of the water-flooding test needs the definition of the initial and boundary conditions.

- *Initial conditions*:
  The oil pressure is fixed at 100 kPa but the water pressure is unknown. As the sample is quite oil saturated, the initial suction may be estimated using the retention curve. If an initial suction of 3 MPa is chosen, it corresponds to a water pressure equal to -2.9 MPa and water saturation equal to 1.23%.
  The initial total stress state is isotropic at a level of 18 MPa.
- *Boundary conditions*:
  At the bottom of the sample, the water pressure is brought to 0.9 MPa. The oil can go out the sample at the upper part where oil pressure is fixed at 100 kPa. The boundary condition for the water at top of the plug is difficult to define: if the boundary is considered as impervious, no water goes out of the sample even if the water front reaches the top; if the water pressure is fixed at the top, the pressure will remain at the initial value. A boundary element was developed for this problem: the boundary is impermeable when the pressure is lower than a
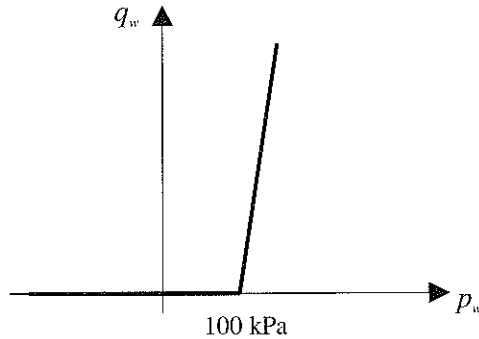
Figure 20. Boundary condition for water at the top of the sample.

given value. In our case, the value corresponds to the atmospheric pressure. Figure 20 defines the relation between the water outflow q_w and the water pressure at the top of the sample. Two types of modelling were performed: a one-dimension axisymetric case and a two-dimension axisymetric case. The one-dimension model is useful to perform a sensitivity study.

The permeability coefficients are defined by relation (44). When the sample is oil saturated according to this relation, the water relative permeability coefficient tends to zero. For a numerical reason, the permeability may not be null and a residual minimum value of the permeability coefficient is defined. This coefficient was proved being important. Indeed, numerical problems can appear due to the severe variation of saturation linked to the shape of the retention curve. In that case, the saturation degree, and therefore the permeability which is a function of saturation, can vary deeply from one element to another.

If a too low value is chosen for this coefficient, the pressure response presents oscillations. Satisfactory numerical results cannot be obtained by using different integration schemes (implicit or Galerkin) and different numbers of elements. A minimum relative permeability value of 0.01 was proved being satisfactory.

The computations show clearly that the flow is a one-dimension problem. However, the stress and strain fields are bi-dimensional. Indeed, when collapse appears near the water front, the sample is no more cylindrical.

Figure 21 shows the water front, which divides the sample into two parts. The lower part was reached by the water front corresponding to water saturation near 70% and porosity of about 38%, whereas the upper part remains near the initial state.

In Figure 22 the mean stress and the axial stress in the sample are shown. It is observed that when the chalk is reached by the water front, the axial strain is compressive with a value of about 2.5% and the axial deformation in the oil-saturated part is a little extensive, about 0.25%. This result is consistent with the porosity change in Figure 21.

The comparison of the numerical results with the experimental data is shown in Figure 23. The injected water volume evolution is similar (Figure 23(a)). After 3500 s, the water front reaches the top; no more oil is driven out of the sample and the water is produced at the top. The saturation profile (Figure 23(b)) shows clearly the water front displacement and the final saturation of 70%.

The computed axial strains at the four gauges present a small swelling followed by a severe collapse of around 2.5% (Figure 23(c)). The experiment value of strain stops at 1%, which
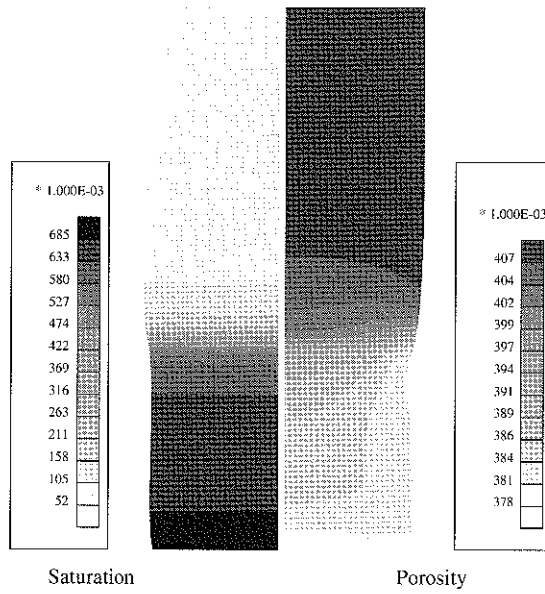
Saturation   Porosity

Figure 21. Water saturation and porosity in the sample.
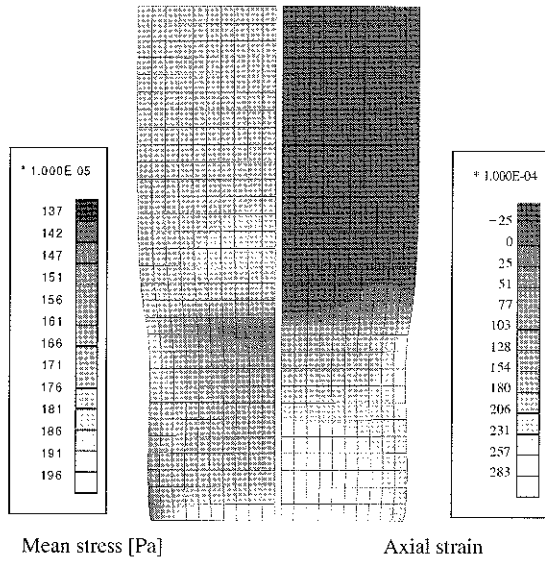

Mean stress [Pa]   Axial strain

Figure 22. Mean stress and axial strain in the sample.

corresponds to the gauge failure. Assuming a piston-like displacement of the water front. Figure 23(d) shows that the compressive strains (measured by gauges) appear when the water front reaches the gauges.

(a) Volume evolution

(b) Saturation profile

(c) Axial deformation evolution
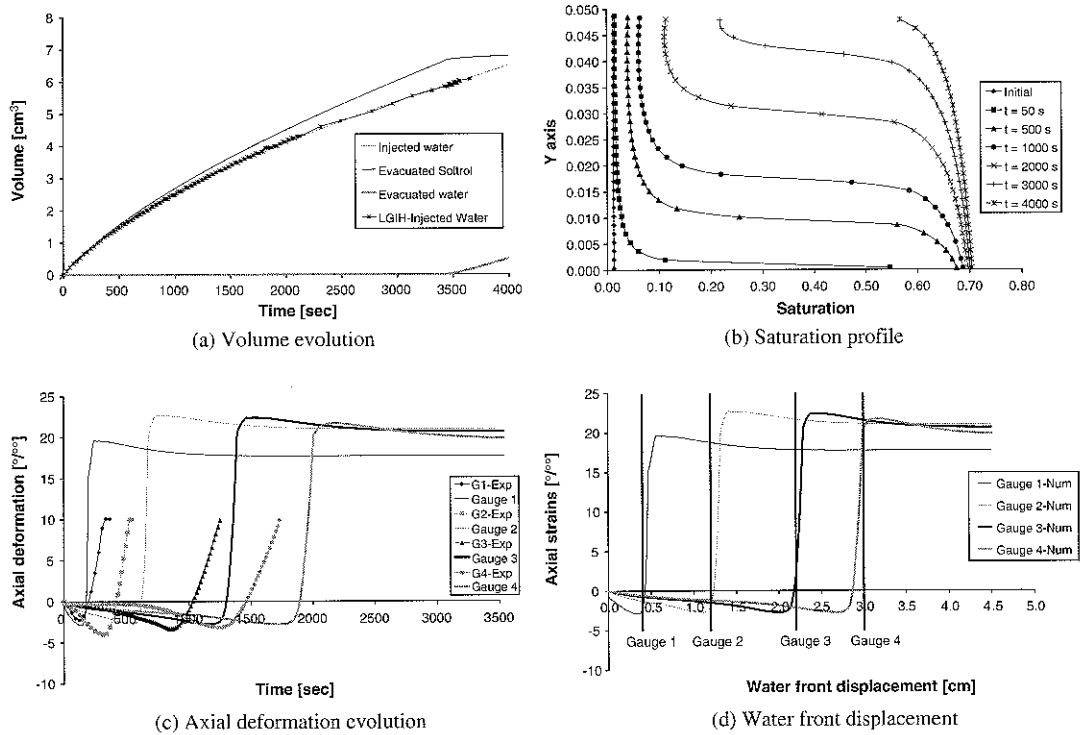

(d) Water front displacement

Figure 23. Numerical simulation of the water-flooding test.

The good consistence obtained between the numerical simulation and the experimental responses shows the validation of the developed model for describing the chalk behaviour during water injection.

6. CONCLUSIONS

A multimechanism model is developed to describe the chalk behaviour during water flooding. The oil–water suction effects are taken into account by integrating the Barcelona model for unsaturated soils in the model.

Experimental results obtained in the Pasachalk project or found in the literature were used to define the parameters. A detailed description of the procedure for the determination of the mechanical parameters was given, which is based on triaxial and oedometer tests results. The obtained values of the parameters are discussed and slightly modified in order to define a set of parameters representing better the chalk behaviour.

The comparison between experimental and numerical results were performed in two levels: triaxial and oedometric tests, and water-flooding test. Satisfactory results were generally obtained, showing the pertinence of the model for the chalk compaction problem due to water injection.

ACKNOWLEDGEMENTS

REFERENCES

1. Delage P, Schroeder C, Cui YJ. Subsidence and capillary effects in chalk. *Proceedings of the Eurock 96*, Turin, 1996; 1291–1298.
2. Masson P, Laurent LJ, D'Heur M. La géologie, de la mer du Nord, Bilan de 15 années d'exploitation pétrolière. *Hommage à Léon Calembert*, Georges, (ed.). Thone: Liége, 1980; 147–181.
3. Alonso EE, Gens A, Josa A. A constitutive model for partially saturated soils. *Géotechnique* 1990; **40**(3):405–430.
4. Bolzon G, Schrefler BA. State surfaces of partially saturated soils: an effective pressure approach. *Appl. Mech. Rev,* American Society of Mechanical Engineers, October 1995; **48**(10):643–649.
5. Monjoie A, Schroeder C, Prignon P, Yernaux C, da Silva F, Debande G. Establishment of constitutive laws of chalk and long term tests. *Proceedings of the 3rd Sea Chalk Symposium*. Copenhagen, June 1990.
6. Shao JF, Henry JP. Development of an elastoplastic model for porous rock. *International Journal of Plasticity* 1991; **7**:1–13.
7. Plischke B, Pisarsky L. Numerical simulation of the stress field close to a producing well. *Proceedings of the 3rd Sea Chalk Symposium*, Copenhagen, June 1990.
8. Papamichos E, Brignoli M, Santarelli FJ. An experimental and theoretical study of partially saturated collapsible rock. *Mechanics of Cohesive-Frictional Materials* 1997; **2**:251–278.
9. Brignoli M, Santarelli FJ, Righetti C. Capillary phenomena in an impure chalk. *Proceedings of the Eurock'94*, Delft, 1994.
10. Piau JM, Maury V. Basic mechanical modelisation of chalk/water interaction. *Proceedings of the 1st International Conference on Unsaturated Soils*, Paris, 1995.
11. Piau JM, Maury V. Mechanical effects of water injection on chalk reservoirs. *Paper SPE/ISRM* 28133, *EUROCK*, 1994.
12. Maury V, Piau JM, Halle G. Subsidence induced by water injection in water sensitive reservoir rocks: the example of Ekofisk. *Proceedings of the 5th North Sea Chalk Symposium*, Reims, October 1996.
13. Homand S, Shao JF. Mechanical behaviour of a porous chalk and effect of saturating fluid. *Mechanics of Cohesive-Frictional Materials* 2000; **5**:583–606.
14. Plischke B. Some aspects of numerical simulation of water-induced chalk compaction. *JCR5 Proceedings of the 5th North Sea Chalk Symposium*, Reims, October 1996.
15. Monjoie A, Schroeder C, Da Silva F, Debande G, Halleux L, Detiège C, Poot B. Mechanical behaviour of chalks. *Proceedings of the North Sea Chalk Symposium*, Stavanger, 1985.
16. Da Silva F, Monjoie A, Schroeder C, Prignon P, Yernaux C, Debande G. Establishment of constitutive laws of chalks and long term tests. *Third North Sea Chalk Symposium*, Copenhaegen, 1990.
17. Andersen MA. *Petroleum Research in North Sea Chalk—Public*. Rogaland Research: Stavanger, 1995.
18. Delage P, Suraj De Silva GPR, Vicol T. Suction controlled testing of non saturated soils with an osmotic consolidometer. *Proceedings of the 7th International Conference on Expansive Soils*, Dallas, 1992; 206–211.
19. Cui YJ. Etude du comportement d'un limon compacté non saturé et de sa modélisation dans un cadre élasto-plastique. *Thèse de doctorat de l'Ecole Nationale des Ponts et Chaussées*, 1993; 297.
20. Schroeder C, Shao JF. Plastic deformation and capillary effects in chalks. *Proceedings of the 5th North Sea Chalk Symposium*, Reims, 1996.
21. Simo JC, Hughes TJR. Computational Inelasticity. *Interdisciplinary Applied Mathematics* 1998; **7**:198–218.
22. Van Eekelen HAM. Isotropic yield surfaces in three dimensions for use in soil mechanics. *International Journal for Numerical and Analytical Methods in Geomechanics* 1980; **4**:98–101.
23. Barnichon JD. Finite element modelling in structural and petroleum geology. *Thèse de doctorat, MSM*, Université de Liége 1998; 186.
24. Risnes R, Korsnes RI, Vatne TA. Tensional strength of chalks in direct and Brazilian tests. *Proceedings of the 9th International Congress on Rock Mechanics*, Paris. Balkema: Rotterdam, 1999.
25. Simo JC, Taylor RL. Consistent tangent operators for rate-independent elastoplasticity. *Computer Methods in Applied Mechanics and Engineering* 1985; **48**:101–118.
26. Alonso EE, Alcoverro J. CATSIUS CLAY Project—calculation and testing of behaviour of unsaturated clay as barrier in radioactive waste repositories. *Publicacion tecnica num.* 10/99, 11/99 & 12/99 ENRESA, Madrid, 1999.
27. Olivella S, Gens A, Carrera J, Alonso EE. Numerical formulation for a simulator (CODE_BRIGHT) for the coupled analysis of saline media. *Engineering Computations* 1996; **13**(7):87–112.

28. Thomas HR, He Y. Analysis of coupled heat, moisture and air transfer in a deformable unsaturated soil. *Géotechnique* 1995; **45**(4):677–689.
29. Fredlund DG, Rahardjo H. *Soil Mechanics for Unsaturated Soils*. Wiley-Interscience Publication, John Wiley & Sons Inc. New York, 1993.
30. Bear J. *Dynamics of Fluids in Porous Media*, American Elsevier Environmental Science Series. Elsevier: New York, 1972.
31. Ebeltoft E, Nordtvedt JE, Sylte A, Oxnevad IEI. Two- and three-phase relative permeabilities and capillary pressures in chalks. *JCR5 Proceedings of the 5th North Sea Chalk Symposium*, Reims, 1996.
32. Brooks RH, Corey AT. *Hydraulic Properties of Porous Media*. Hydrology papers, Colorado State University, 1964.
33. Schroeder C, Bois AP, Maury V, Hallé G. Water/chalk (or collapsible soil) interaction: Part II. Results of tests performed in laboratory on Lixhe chalk to calibrate water/chalk models. *SPE/ISRM Eurock'98 Trondheim (SPE 47587)*, 1998.